Fragmentation of atomic systems

John L. Bohn* and U. Fano
Physics Department and James Franck Institute, University of Chicago, Chicago, Illinois 60637
(Received 16 November 1995)

We report recent progress toward a nonperturbative formulation of many-body quantum dynamics that treats all constituent particles on an equal footing. This formulation is capable of detailing the evolution of a system toward the diverse fragments into which it can break up. We illustrate the general concept with the simple example of the simultaneous excitation of both electrons in a helium atom. [S1050-2947(96)07206-X]

PACS number(s): 31.10+z

I. INTRODUCTION

Chemical reactions proceed generally with reactants converging to form a ''complex'' (or ''transition state''), followed by fragmentation of the complex into alternative channels. The fragmentation process may begin with the complex in a compact state, whose radius r depends on a balance between the kinetic energy of confinement within the radius r and the Coulomb interaction between nuclei and electrons less than a distance r apart. The kinetic energy arising from particle concentration in a small volume is generally represented by a centrifugal potential that decreases as the inverse radius squared. This potential leads to radial expansion until the Coulomb interaction, inversely proportional to the radius, becomes dominant, thus allowing the system to evolve toward alternative fragmentation channels.

These circumstances are generally familiar. The same dynamics applies, perhaps less familiarly, to the excitation of atomic systems initially in their ground state and then excited, e.g., by light absorption. The sudden absorption of energy enables the system to sample larger centrifugal fields, thus breaking the ground state's stability and causing the radius to expand toward fragmentation, typically in a channel with an electron (or a few electrons) separate from a residual core. This situation often differs in that the energy absorbed from radiation does not suffice to achieve full fragmentation, achieving instead a new equilibrium characteristic of an excited state. This remark intends to stress that fragmentation processes occur whether or not the available energy suffices to reach full separation of a system, including thus a large fraction of all physicochemical phenomena.

Note also that the formation of a complex with sufficient energy to expand toward fragmentation is basically reciprocal to fragmentation itself. Accordingly it was stressed earlier [1] that the study of fragmentation *per se* encompasses much of atomic and molecular physics.

Quantum mechanical scattering theory often constructs ''Jost'' matrices that connect whole sets of alternative compact ''c'' states of each system with alternative fragmented ''f'' states, matrices indicated here by J_{fc} [2]. A standing wave function is then represented, in the limit of large radial distances, by $\sin(k_f r)J_{fc}$. More conveniently one separates outgoing and incoming components of this function in the form

$$e^{ik_f r}J^{+}_{fc}, \quad e^{-ik_f r}J^{-}_{fc}. \tag{1}$$

The matrices J^{+} and J^{-} are complex conjugate when the energy suffices to achieve full fragmentation, that is for energetically ''*open*'' channels. For the ''*closed*'' channels instead, the k_f values are imaginary, whereby one component of Eq. (1) converges exponentially as $r\rightarrow\infty$, and the other diverges. The Jost matrices serve to construct scattering matrices

$$S_{f'f}=\sum_c J^{+}_{f'c}\left[\frac{1}{J^{-}}\right]_{cf} \tag{2}$$

for open channels. Analogous matrices occur for closed channels, as detailed in Ref. [1].

Substantial evidence, outlined, e.g., in [3], indicates that the values of Jost matrices, derived from experiment or calculated by solving relevant Schrödinger equations, actually receive major contributions at localized values of the radial distance. The Jost matrices typically fail to exploit this circumstance, being computed at a single radial distance only. A main focus here will therefore be to extract the detailed *evolution* of Jost matrices from their short- to long-range behaviors. More precisely, the present treatment yields a set of approximate quantum numbers, appropriate to the near separability of each region of space, that interpolate smoothly between the c and f limits as the system evolves. This study continues a previous preliminary report [4], extending its results to higher energies.

II. FORMULATION

According to Ref. [1], atomic and molecular states are best described in the framework of scattering theory and globally for the whole system under consideration rather than primarily as aggregates of independent constituents. For purposes of introduction, we consider first the radial evolution of a single particle scattered by a potential well.

A. Elementary example

Separation of variables holds for spherically symmetric wells, yielding partial-wave solutions for each orbital momentum eigenfunction of the form $\Psi_{lm}(r,\theta,\varphi)$

*Present address: JILA, Campus Box 440, University of Colorado, Boulder, CO 80309.

$=F_{lm}(r)Y_{lm}(\theta,\varphi)$. Asymmetries of the potential well allow separation to hold only in the limits of small or large radial distances. Thus we write

$$\Psi_{l_0m_0}(r,\theta,\varphi)\to r^{l_0+1}Y_{l_0m_0}(\theta,\varphi) \quad \text{as } r\to 0, \tag{3a}$$

with subscripts ''l_0m_0'' to indicate the zero-r behavior, i.e., the ''c'' limit. At larger radial distances, the wave function is expanded into a series of spherical harmonics,

$$\Psi_{l_0m_0}(\vec{r})=\sum_{lm} F_{l_0m_0,lm}(r)Y_{lm}(\theta,\varphi). \tag{3b}$$

The coefficients of this expansion are then determined by solving a system of coupled *ordinary* differential equations governing the $F_{l_0m_0,lm}(r)$.

Separability prevails again, however, beyond the rim of the potential well, i.e., at $r>r_0$, where each independent wave function $\Psi^{\rho}(\vec{r})$ factors into the product of a radial and of an angular function,

$$\sum_{l_0,m_0} A^{\rho}_{l_0m_0}\Psi_{l_0m_0}(\vec{r})=\sin(k_\rho r+\delta_\rho)\sum_{l,m} b^{\rho}_{lm}Y_{lm}(\theta,\varphi)$$

$$\text{for } r>r_0. \tag{4}$$

The phase shift δ_ρ and the coefficients b^{ρ}_{lm} in this equation represent, respectively, the eigenphase shift and the eigenvector of the matrix (2) that represents the electron's scattering by the potential well.[1] These parameters have no r dependence, reflecting the entire effect of the potential well on the scattered particle. For long-ranged potentials, e.g., Coulomb potentials, an equivalent separability prevails anyhow, in the asymptotic limit $r\to\infty$ [5].

B. Displaying the progression of phase shifts

A major contribution towards describing the evolution of atomic systems from their compact to their fragmented states stems from a suggestion in the mid-1960's, which was hardly ever implemented since that time [6]. Its centerpiece consists of working out how each phase shift attains its value δ_ρ beyond the rim of a potential well in the course of propagation from the center to the rim of the potential well. To this end in Ref. [6] the idea was conceived of *truncating* the potential well at a sequence of mock rims with intermediate radii $0\leqslant r\leqslant r_0$, a method now dubbed as ''invariant imbedding'' [7].

Not only each mock phase shift δ_ρ, but also its corresponding mock eigenvector $\langle\rho|lm\rangle$ is evaluated at each radius r, being thus mapped as a function of that radius. This procedure establishes a direct link from the zero value of δ_ρ as $r\to 0$ (where the eigenvector $\langle\rho|lm\rangle$ reduces to its single nonzero component $\langle\rho|l_0m_0\rangle$), to its actual value at the rim $r=r_0$. The procedure appears to have been first implemented in a study on diatomic molecules [8], where r stood for the internuclear distance, and more recently for a H atom in a magnetic field [9], as well as for the doubly excited states of helium [10]. These results compute phase *shifts*, which are tied to the set of reference functions selected. In the following we will describe instead a more flexible procedure, first elaborated in [4], that determines eigenchannels of *total phase*, which prove independent of the radial basis in which they are computed.

C. Multiparticle treatment

Returning now to our task of formulating the solution of the Schrödinger equation for multiparticle systems, we must first establish an appropriate system of coordinates. We take a cue from the simplest example of the He atom, where radial correlations between the two electrons have long been represented by changing the Cartesian coordinate pair (r_1,r_2) into the polar coordinate pair (R,α). Similarly, the set of multiparticle position coordinates $\{\vec{r_1},\vec{r_2},\ldots,\vec{r_N}\}$ is represented by a single $3(N-1)$-dimensional vector $\vec{R}$ with origin at the system's center of mass, for example, at the nucleus of a single atom. This vector is then represented in multidimensional polar hyperspherical mass-weighted coordinates $\vec{R}\equiv\{R,\hat{R}\}$ with

$$R=\sqrt{\frac{\Sigma_i m_i r_i^2}{M}}, M=\sum_i m_i, \sum_i m_i\vec{r_i}=0. \tag{5}$$

This multidimensional notation leads us to replace the expansion (3b) in spherical harmonics with an expansion of the wave function $\Psi(\vec{R})$ into hyperspherical harmonics $Y_{\lambda\vec{\mu}}(\hat{R})$, eigenfunctions of the hyperangular Laplacian $\Delta_{\hat{R}}$, with eigenvalue $\lambda(\lambda+3N-5)$; see, e.g., Ref. [11]. Here $\vec{\mu}$ stands for a set of quantum numbers conjugate to the angular coordinates $\hat{R}$. Many parametrizations of $\hat{R}$ and $\vec{\mu}$ exist, which we need not specify here. There results the expansion

$$\Psi_{\lambda_0\vec{\mu_0}}(\vec{R})=\sum_{\lambda,\vec{\mu}} F_{\lambda_0\vec{\mu_0},\lambda\vec{\mu}}(R)Y_{\lambda\vec{\mu}}(\hat{R}). \tag{6a}$$

The analogue of Eq. (3a), representing the hyper-radial wave near $R=0$, then reads

$$F_{\lambda_0\vec{\mu_0},\lambda\vec{\mu}}(R)\to R^{\lambda_0+(3N-4)/2}\delta_{\lambda_0\vec{\mu_0},\lambda\vec{\mu}} \quad \text{as } R\to 0. \tag{6b}$$

The expansion (6a) leads to the set of close-coupled radial Schrödinger equations

$$\frac{d^2}{dR^2}F_{\lambda_0\vec{\mu_0},\lambda\vec{\mu}}(R)+\sum_{\lambda'\vec{\mu'}}\langle\lambda\vec{\mu}|k^2(R)|\lambda'\vec{\mu'}\rangle$$

$$F_{\lambda_0\vec{\mu_0},\lambda'\vec{\mu'}}(R)=0, \tag{7}$$

with the squared-wave-number matrix

[1]The wave function of the scattered electron is represented, outside the potential well, in the generic form $\sin(k_\rho r)Y_{lm}(\theta,\varphi)+\cos(k_\rho r)\Sigma_{l'm'}Y_{l'm'}(\theta,\varphi)K_{l'm',lm}$. The ''reaction matrix'' K is represented, in turn, through its eigenvalues and eigenvectors as $\Sigma_{\rho'}\langle l'm'|\rho'\rangle\tan\delta_{\rho'}\langle\rho'|lm\rangle$. Multiplying the wave function, on its right, by $\langle lm|\rho\rangle\cos\delta_\rho$ and rewriting the eigenvector $\langle lm|\rho\rangle\cos\delta_\rho$ as b^{ρ}_{lm} yields the wave function (4).

$$\langle \lambda\vec{\mu}|k^2(R)|\lambda'\vec{\mu'}\rangle = \left[2ME - \frac{[\lambda+(3N-5)/2]^2-\frac{1}{4}}{R^2}\right] \times \delta_{\lambda\vec{\mu},\lambda'\vec{\mu'}} + \frac{\langle \lambda\vec{\mu}|Z(\hat{R})|\lambda'\vec{\mu'}\rangle}{R} + \cdots . \quad (7')$$

Here $Z(\hat{R})/R$ represents the Coulomb potential energy of the interacting constituents, evaluated at a fixed hyper-radius R. The ellipses at the end of Eq. (7′) stand for possible additional terms of the k^2 matrix corresponding to Hamiltonian terms for spin-orbit or relativistic corrections. The ability of this equation to include such effects appears very important because it bypasses the previous need to introduce them by perturbative treatments rather than directly in the basic equation.

D. *R*-matrix equation

Solving our multidimensional Eq. (7) requires us to modify our initial treatment of a single particle in a potential well, insofar as the potential well was surrounded, beyond its rim, by a region without potential. A phase shift was then introduced to represent the wave function's phase generated by the well ''in addition'' to the phase that would have resulted from the wave function's propagation free of potential.

The formulation of Eq. (7) leaves instead the range of integration unspecified, providing a single boundary condition at $R=0$. We deal thus with solving the equation over successively increasing finite ranges of R, analogous to the successive radii r considered in Sec. II B. We impose an appropriate boundary condition at each selected value of R. The condition seeks eigenfunctions that display a *uniform ''eigenphase''* over the whole hyperspherical surface of radius R, much as the relevant eigenfunctions in Sec. II A or II B sought constant phase shifts beyond the well's rim at r_0. To fulfill this requirement, one diagonalizes, over the surface, an R matrix $\mathcal{R}$ that represents the normal logarithmic radial derivative of the solution $F(R)$ of Eq. (7), namely,

$$\langle \lambda\vec{\mu}|\mathcal{R}(R)|\lambda'\vec{\mu'}\rangle = \sum_{\lambda_0\vec{\mu_0}} \left[\frac{dF}{dR}\right]^{-1}_{\lambda\vec{\mu},\lambda_0\vec{\mu_0}} F_{\lambda_0\vec{\mu_0},\lambda'\vec{\mu'}}(R) = \sum_{\rho} \langle \lambda\vec{\mu}|\rho\rangle \tan\phi_\rho(R) \langle \rho|\lambda'\vec{\mu'}\rangle . \quad (8)$$

Solving Eq. (7) within this frame proceeds, as in Ref. [4], by seeking $\mathcal{R}$ directly—instead of the function $F(R)$ itself, by transforming the second-order Eq. (7) into a pair of first-order ''variable phase'' equations for the eigenvalue $\phi_\rho(R)$ and eigenvectors $\langle \rho|\lambda\vec{\mu}\rangle$ of the $\mathcal{R}$ matrix. The relevant equations read [4]

$$\frac{d\phi_\rho}{dR} = \cos^2\phi_\rho + \langle \rho|k^2(R)|\rho\rangle \sin^2\phi_\rho , \quad (9a)$$

$$\frac{d\langle \rho|\lambda\vec{\mu}\rangle}{dR} = \sum_{\rho'\neq\rho} \frac{\sin\phi_\rho \langle \rho|k^2(R)|\rho'\rangle \sin\phi_{\rho'}}{\sin(\phi_\rho-\phi_{\rho'})} \langle \rho'|\lambda\vec{\mu}\rangle . \quad (9b)$$

Thus each channel's eigenphase ϕ_ρ evolves nearly independently, driven by an effective channel potential embodied in the diagonal portion of the squared channel wave number. Coupling between different ρ channels is instead embodied in Eq. (9b), whose denominator vanishes whenever two of the eigenphases ϕ_ρ become degenerate, i.e., coincide *modulo* π. The resulting singularity of the equation yields an ''avoided crossing'' of the corresponding plots of the eigenphase pair. These plots bend then, more or less sharply, depending on the numerator's value, generating a localized disturbance of the relevant propagation channels, as will be very apparent in Sec. III.

The eigenvectors $\langle \rho|\lambda\vec{\mu}\rangle$ serve to connect smoothly the $|\lambda_0\vec{\mu_0}\rangle$ channels at small R to the fully coupled $\langle \rho|$ channels at larger R, i.e., they transform between the ''c'' and ''f'' channels referred to in the Introduction. Note, however, that Eqs. (9) describe only the ''phase'' portion of a phase-amplitude method. Full scattering solutions to the Schrödinger equation would require solution of a further set of ''amplitude equations,'' which would remix the ρ eigenchannels. We emphasize, however, that the eigenphases $\phi_\rho(R)$ contain information on both the energy levels and autoionization widths of the doubly excited states of helium. This circumstance, detailed in [4], arises because the eigenphases adequately represent the hyper-radial nodal structure of the wave function. Evaluation of the *exact* energies and widths would require evaluation of channel coupling in the $R\to\infty$ limit, either by continuing the integration of Eqs. (9), or by an ''elimination of closed channels'' in the framework of quantum defect theory. We have not attempted this evaluation here, since our interest lies in the short-range evolution of the fragmentation channels.

E. Numerical computation of the eigenphases

In principle, the expansion (6a) of a stationary state wave function into hyperspherical harmonics is valid, since the harmonics form a complete set. In practice, however, the convergence is very slow even at moderate values of R [12]. Thus while the harmonic expansion sufficed for the limited application of Ref. [4], an alternative expansion proves necessary for the higher energies discussed here. Note that the R matrix described above identifies its own eigenchannels in a basis-independent way; a specific choice of basis functions serves only to simplify calculation.

To this end, a useful set of basis functions is afforded by the well-known adiabatic approximation, modeled on the born-Oppenheimer approximation of molecular physics [13]. This approximation treats the hyper-radius R as a ''slow'' coordinate, diagonalizing then the operator $k^2(R)$ of Eq. (7′) to yield a set of potential curves $U_\nu(R)$ and adiabatic angular functions $\Phi_\nu(R;\hat{R}) = \Sigma_{\lambda,\vec{\mu}} c^\nu_{\lambda\vec{\mu}}(R) Y_{\lambda\vec{\mu}}(\hat{R})$:

$$\sum_{\lambda',\vec{\mu}'}\left[\frac{[\lambda+(3N-5)/2]^2-\frac{1}{4}]}{R^2}\delta_{\lambda\vec{\mu},\lambda'\vec{\mu}'}-\frac{\langle\lambda\vec{\mu}|Z(\hat{R})|\lambda'\vec{\mu}'\rangle}{R}\right]c^{\nu}_{\lambda'\vec{\mu}'}(R)=U_{\nu}(R)c^{\nu}_{\lambda\vec{\mu}}. \tag{10}$$

Standard procedures exist for calculating these potential curves very accurately [14], along with the antisymmetric matrices $P_{\nu\nu'}$ that describe their nonadiabatic couplings:

$$P_{\nu\nu'}=\int d\hat{R}\Phi_{\nu}(R;\hat{R})\frac{\partial}{\partial R}\Phi_{\nu'}(R;\hat{R}). \tag{11}$$

Cast in these terms, Eq. (9a) remains unchanged, but (9b) is complemented by the P matrix as follows:

$$\frac{d\langle\rho|\nu\rangle}{dR}=\sum_{\nu'}\langle\rho|\nu'\rangle P_{\nu'\nu}+\sum_{\rho'\neq\rho}\frac{\sin\phi_{\rho}k^2_{\rho\rho'}\sin\phi_{\rho'}}{\sin(\phi_{\rho}-\phi_{\rho'})}\langle\rho'|\nu\rangle. \tag{9b$'$}$$

The results in the next section were computed by directly integrating Eqs. (9a) and (9b$'$), which, although nonlinear, prove remarkably stable, producing results in fair agreement with more elaborate calculations. Coupling only the lowest ten adiabatic channels proved sufficient to obtain the results presented here.

III. APPLICATION TO DOUBLY EXCITED HELIUM ^1S STATES

The main application of Sec. II has been carried out in Ref. [15] to the simple case of ^1S states of helium, with boundary conditions at $R=0$ classified by a set of hyperspherical quantum numbers appropriate to a pair of electrons in the field of an infinitely heavy nucleus. These are the orbital momenta of each electron l (equal to one another for the S state), and an additional n, representing the number of nodes of the wave function factor corresponding to oscillations of the ratio between the electrons' radial coordinates, $r_2/r_1=\tan\alpha$. This pair of quantum numbers determines the value of the λ quantum number introduced in Sec. II, namely, $\lambda=2(l+n)$.

The equation pair (9a), (9b$'$) was integrated numerically at a sequence of increasing energies E, in the range of 57–74 eV above the helium ground state, corresponding to several of the lower-lying double excitations of helium. We describe here primarily the behavior of the eigenphases ϕ_{ρ}, implying many corresponding features of their associated eigenvectors $\langle\rho|$.

Figure 1 displays a set of eigenphases $\phi_{\rho}(R)$, with modest ρ values, plotted mod π over the range of R up to 16 a.u., calculated at energies E about 21 eV below the double-ionization threshold, specifically just below (a) and above (b) the lowest doubly excited level, ''$(2s^2)^1S$.'' Dashed lines have been inserted to suggest the ''diabatic'' connection of eigenphases, in the sense of the Landau-Zener treatment of curve crossings [16]. That is, we view initially the eigenphases with similar slopes on either side of a crossing as belonging together. At values of ϕ_{ρ} up to about 0.2π, all crossings do appear diabatic, owing partly to the near-zero

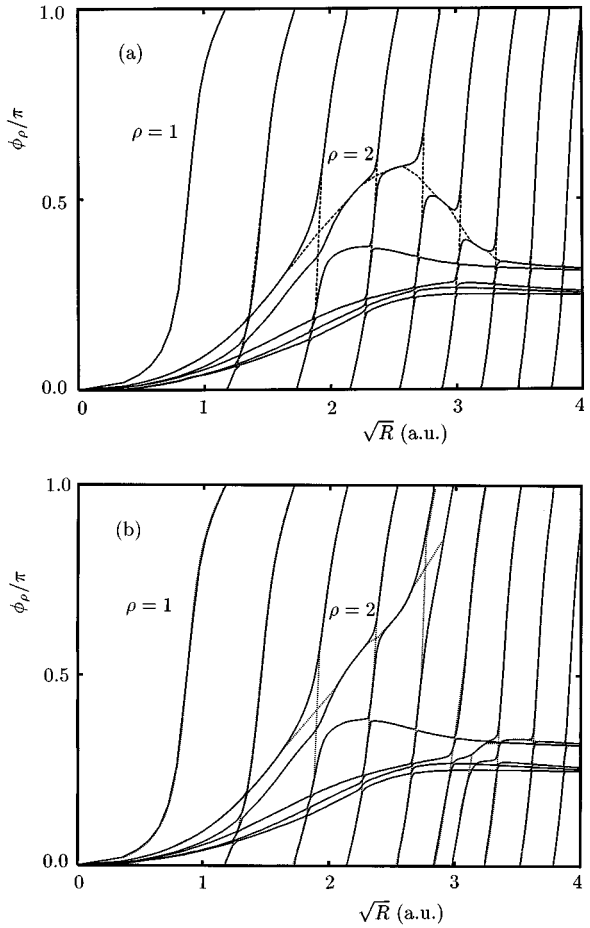

FIG. 1. (a) Eigenphases modulo π, ϕ_{ρ}/π, vs the square root of the hyper-radius, calculated at the total energy $E=57$ eV above the ground state, just below the ''$(2s^2)^1S$'' resonant state of helium. The dashed lines suggest diabatic crossings, as discussed in the text. (b) shows the same set of eigenphases, calculated at a total energy $E=58$ eV above the ground state.

factors $\sin\phi_{\rho}$ in the numerator of the singular term of the Eq. (9b$'$). As expected, the curves start at the origin, with different slopes corresponding to different values of the parameter λ that controls the strength of the centrifugal potential in Eq. (7$'$). The fastest rising curve, corresponding to single-electron ionization, attains the value of π quickly, since the ejected electron travels rapidly, with a kinetic energy above 33 eV. The plot shows this curve emerging repeatedly at the zero ordinate, corresponding to successive multiples of π.

The second most rapidly rising eigenphase, labeled ''$\rho=2$'' in Fig. 1, represents a resonant state with insufficient energy to fragment all the way to $R\rightarrow\infty$. Indeed, this eigenphase reaches π for the first time only at the slightly higher energy of Fig. 1(b); this occurrence of a phase equal to π, i.e., the addition of a radial node in the wave function, signals the resonant energy [4]. Moreover, when viewed as a function of energy at a large fixed value of R, a single eigenphase is seen to rise by $\sim\pi$ within a certain well-defined width (cf. Fig. 6 of Ref. [4]). The energy derivative of this rise yields a Lorentzian line shape centered at an energy $E=57.8$ eV above the helium ground state, with a full width at half maximum of $\Gamma=0.098$ eV, as compared to the accu-

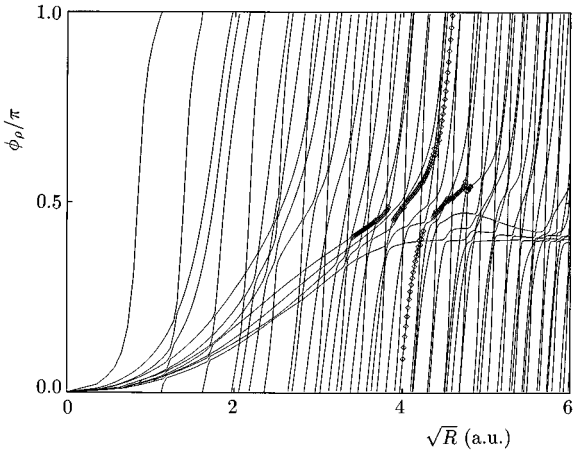

FIG. 2. A set of eigenphases similar to those of Fig. 1, but calculated at an energy of $E=74$ eV above the ground state, near the ''$(4s^2)^1S$'' resonant state of helium. Note the strong diabaticity of most crossings. Nevertheless, there still exist large avoided crossings in the eigenphases, notably the one indicated by the diamond symbols. Such crossings indicate the well-localized regions where the channels interact.

rate calculations of Ho [17], $E=57.8$ eV, $\Gamma=0.125$ eV. Notice that the eigenphases predict too small a width, i.e., a greater stability of the resonant state, indicating a small additional coupling between the resonant and continuum channels at even larger values of R.

For values of ϕ_ρ near $\pi/2$, many crossings are clearly avoided, implying increasing variation of the eigenvectors $\langle\rho|$, according to (9b′). Again following Ref. [16], a more realistic view interprets the eigenvector $\langle(\rho=1)|$ as evolving smoothly into the eigenvector $\langle(\rho=2)|$ as the crossing is traversed from left to right.

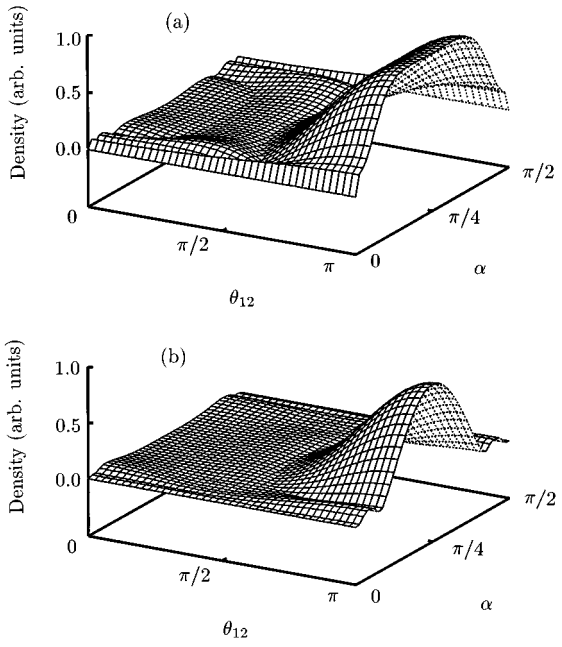

FIG. 3. Electron pair density for a ridgelike R-matrix eigenchannel function evaluated just *before* (a) and *after* (b) the large avoided crossing in Fig. 2. This crossing sharpens the ridge localization of the channel function.

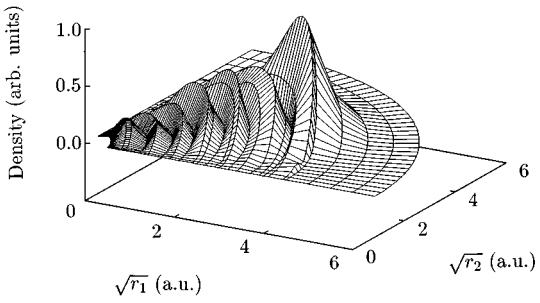

FIG. 4. Electron pair density as defined in Eq. (12), for the ''$(4s^2)^1S$'' resonant state of helium. The absence of nodes in the α coordinate identifies this mode as localized on the potential ridge.

Figure 2 presents an analogue of Fig. 1 for an energy near the ''$(4s^2)^1S$'' resonance. As above, the energy dependence of the eigenphases at large R identifies the energy of the resonance as $E=73.5$ eV above the helium ground state, and its width as $\Gamma=0.046$ eV, as compared to Ho's $E=73.5$ eV and $\Gamma=0.053$ eV [17]. Again, the width predicted by the eigenphases is too small, expressing the missing coupling between bound and continuum states that we have neglected. Notice that many more eigenphases appear here, owing to the much larger number of possible excitations of the atom at this higher energy. Nevertheless, most of these eigenphases rise rapidly through many multiples of π, representing the numerous single ionization channels available at this energy, which are mostly irrelevant to our present discussion of the doubly excited states. The eigenphases serve to *identify* and *separate* the independent excitations, as evidenced by the sharpness of the majority of avoided crossings in Fig. 2. Large avoided crossings occur instead only when interaction between different excitations is inescapable. An example is indicated by the diamond symbols in Fig. 2, which highlight the primary region of interaction where the ''$4s^2$'' state couples to the primary continuum channel into which it autoionizes. The concentration of these crossings in a small range of R (and near $\phi_\rho=\pi/2$) documents the initial expectation that major physical processes arise within a minor fraction of the ranges of relevant variables.

Reference [15] details the rapid evolution of eigenchannels across large avoided crossings of their eigenphases. Figure 3 illustrates this rapid evolution for a particular case, namely, the large avoided crossing near $R=17$ a.u. indicated in Fig. 2. These figures show the electron pair density, plotted versus the angles α and $\theta_{12}=\cos^{-1}(\hat{r}_1\cdot\hat{r}_2)$ for fixed hyper-radii before [Fig. 3(a)] and after [Fig. 3(b)] the crossing. Figure 3(a) shows a channel with density localized near a high potential region, colloquially labeled the ''ridge,'' at equal radial distances ($r_1=r_2$ or $\alpha=\pi/4$) and at $\vec{r}_1$ near $-\vec{r}_2$ [18]. [2] This localization appears unstable, since the density appears flattened in the immediate vicinity of the ridge, indicating its impending approach to lower potential regions.

[2]The name ''ridge'' arises because the effective charge function $Z(\hat{R})$ in Eq. (7′) exhibits a local maximum in the α coordinate at $\alpha=\pi/4$.

Nevertheless, on the other side of the crossing this channel has stabilized on the ridge [Fig. 3(b)]. Wave functions localized on the ridge had been constructed in the past, but the emergence of this localization from the same *ab initio* treatment that localizes single ionization at α values near the ends of their range amounts to a major contribution of Ref. [15].

Finally, Fig. 4 documents more globally the concentration of an eigenchannel on the ridge. We plot here the squared eigenchannel function

$$|\sin\phi_\rho(R)\sum_\nu \Phi_\nu(R;\hat{R})\langle\nu|\rho(R)\rangle|^2$$

$$=|\sin\phi_\rho(R)\sum_{\lambda\vec{\mu}} Y_{\lambda\vec{\mu}}(\hat{R})\langle\lambda\vec{\mu}|\rho(R)\rangle|^2, \qquad (12)$$

analogous to the function (4) in the single-particle case. The function (12) is plotted in the (r_1,r_2) plane, with the angle θ_{12} between the electron directions held fixed at π. This function was constructed at the same energy as the eigenphases of Fig. 2, traversing the large avoided crossings adiabatically, that is, treating them as avoided crossings. The resulting Fig. 4 displays no nodes in the α coordinate, in accordance with a stable localization about the potential ridge.

The quantity being squared in Eq. (12) does not represent a full solution to the Schrödinger equation, since it has yet to be complemented by an R-varying amplitude function. In general, such amplitudes will mix alternative channels having different eigenphases. This mixing is, however, also expected to concentrate near avoided crossings of the eigenphases. Thus, while Fig. 4 fails to identify a physical electron density, it does isolate a significant contribution to the full electron-pair dynamics. Its specific contribution will be the subject of a future report.

IV. DISCUSSION

This paper has summarized the extension of the procedures of Refs. [4,9,15] to realistic *ab initio* applications to multiparticle systems. The main feature of this procedure lies in its systematic utilization of locally separable approximations to solve globally nonseparable problems. Local separability prevails in the limit $R\to 0$ where the centrifugal potential—and thereby rotational invariance—prevails. It prevails even more obviously in the fragmentation limit, where two of the system's elements fall apart. (Details of the fragmentation have been laid out in Ref. [19].) The artifice described in Sec. II B [6] amplifies the implementation of local separability. This procedure affords the future options of enforcing uniformity of parameters other than ϕ_ρ—for instance, $d\phi_\rho/dR$—over constant-R surfaces.

The major pending challenge to the present approach lies in extending its application to systems with increasing numbers of particles. Multielectron atoms have been treated by Cavagnero [20] to the extent of constructing generic matrices of the ''effective charge'' $Z(\hat{R})$ of Eq.(7′). More complex, however, is the task of mastering the dynamical evolution of systems with numerous and diverse particles, as well as that of implementing an adequate development of the systematics and practice of hyperspherical harmonics. The example of the H_2 molecule has been under development in this group for some time, but not yet completed. Extensive efforts have been directed to formulate the geometrical aspects of this undertaking, as well as the systematics of hyperspherical harmonics, whose results remain to be published.

These technical hurdles remain in treating the angular coordinates. On the other hand, the situation in the hyper-radial coordinate is much clearer. In general, rapidly rising eigenphases should represent fairly ''trivial'' fragmentations, such as single ionizations in the present case, or dissociations in the molecular case. At the other extreme, eigenphases that grow slowly belong to ''strongly closed'' channels, which only become important at larger total energies. Therefore only a modest collection of eigenphases in between these extremes yields relevant dynamics in a given energy range. Maps of the eigenphases, and especially their avoided crossings, versus R and E should prove valuable in sorting out fragmentations in many systems.

ACKNOWLEDGMENTS

The research reported here has been supported by the NSF Grant No. Phy 9217874.

[1] U. Fano, Phys. Rev. A **24**, 2402 (1981); **27**, 1208 (1983).
[2] R. G. Newton, *Scattering Theory of Waves and Particles* (McGraw-Hill, New York, 1966).
[3] U. Fano, in *Fundamental Processes of Atomic Dynamics*, edited by J. Briggs *et al.* (Plenum, New York, 1988), pp. 41–48.
[4] J. L. Bohn, Phys. Rev. A **51**, 1110 (1995).
[5] M. J. Seaton, Rep. Prog. Phys. **46**, 167 (1983).
[6] C. Zemach, Nuovo Cimento **33**, 939 (1964); A. Degasperis, *ibid.* **34**, 1667 (1964); F. Calogero, *Variable Phase Approach to Potential Scattering* (Academic, New York, 1967).
[7] R. Bellman and G. M. Wing, *An Introduction to Invariant Imbedding* (Wiley-Interscience, New York, 1975); B. R. Johnson, J. Comput. Phys. **13**, 445 (1973).
[8] S. J. Singer *et al.*, J. Chem. Phys. **77**, 1942 (1982).
[9] U. Fano and E. Y. Sidky, Phys. Rev. A **45**, 4776 (1992); E. Y. Sidky, *ibid.* **47**, 2812 (1993).
[10] J. L. Bohn, Phys. Rev. A **49**, 3761 (1994).
[11] Y. F. Smirnov and K. V. Shitikova, Fiz. Elem. Chastits. At. Yadra. **8**, 847 (1977) [Sov. J. Part. Nucl. **8**, 344 (1977)].
[12] J. Macek (private communication). The poor convergence of hyperspherical harmonics for three-electron atoms is demonstrated in C. H. Greene and C. W. Clark, Phys. Rev. A **30**, 2161 (1984).
[13] J. H. Macek, J. Phys. B **1**, 831 (1968); C. D. Lin, Adv. At. Mol. Phys. **22**, 77 (1986).
[14] H. R. Sadeghpour, Phys. Rev. A **43**, 5821 (1991).

[15] J. L. Bohn, Ph.D. thesis, University of Chicago, 1995 (unpublished).
[16] C. Zener, Proc. R. Soc. London A **137**, 696 (1932); L. Landau and E. M. Lifshitz, *Quantum Mechanics: Non-Relativistic Theory*, 2nd ed. (Pergamon, Oxford, 1965), p. 322.
[17] Y. K. Ho, Phys. Rev. A **34**, 4402 (1986).
[18] U. Fano, Rep. Prog. Phys. **46**, 97 (1983).
[19] U. Fano, J. Phys. Chem. **99**, 15624 (1995).
[20] M. Cavagnero, Phys. Rev. A **30**, 1169 (1984); **33**, 2877 (1986); **36**, 523 (1987).